Near- and sub-barrier fusion of the ^{7}Be + ^{58}Ni system

E. Martinez-Quiroz, E. F. Aguilera,* D. Lizcano, P. Amador-Valenzuela,† and H. García-Martínez
Departamento de Aceleradores, Instituto Nacional de Investigaciones Nucleares, Apartado Postal 18-1027, Código Postal 11801, México, Distrito Federal, México

J. J. Kolata, A. Roberts,‡ L. O. Lamm,§ and G. Rogachev‖
Physics Department, University of Notre Dame, Notre Dame, Indiana, 46556-5670, USA

V. Guimarães
Instituto de Fisica, Universidade de Sao Paulo, P. O. Box 66318, 05389-970, Sao Paulo, SP, Brazil

F. D. Becchetti, A. Villano,¶ M. Ojaruega, M. Febbraro, Y. Chen,** and H. Jiang
Physics Department, University of Michigan, Ann Arbor, Michigan, 48109-1040, USA

P. A. DeYoung
Department of Physics, Hope College, Holland, Michigan, 49423-9000, USA

G. F. Peaslee
Department of Chemistry, Hope College, Holland, Michigan, 49423-9000, USA

(Received 24 March 2014; revised manuscript received 7 July 2014; published 29 July 2014)

Evaporation proton yields were measured for the fusion of the radioactive proton-rich nucleus ^{7}Be onto a ^{58}Ni target at six near-barrier energies. Total fusion cross sections were deduced by using calculated proton multiplicities. The resulting fusion excitation function shows a considerable enhancement with respect to calculations for a bare potential, even for energies above the Coulomb barrier. Inelastic couplings can account for the enhancement at the highest energy. Total fusion channels nearly saturate the total reaction cross section in the measured energy region. Comparison with previous results scaled appropriately for ^{7}Be + (^{27}Al,^{238}U) shows good agreement.

DOI: 10.1103/PhysRevC.90.014616 PACS number(s): 25.60.Pj, 25.70.Jj

I. INTRODUCTION

The properties of interactions with weakly bound projectiles have attracted much attention lately [1,2]. The near-barrier fusion process for these nuclei, in particular, has been the subject of many recent studies, both experimental and theoretical. Within the subfield of fusion with radioactive nuclei, the pioneering work by the Dubna group [3] triggered a series of measurements involving the neutron-halo nucleus ^{6}He. In particular, important work was reported in Ref. [4], where an excitation function for the near and sub-barrier fusion of the ^{6}He + ^{209}Bi system was measured. From these as well as from later measurements for other neutron-halo systems, it has been shown that the total fusion cross sections are suppressed with respect to expectations for energies above the barrier [5,6]. Below the barrier, these systems exhibit a fusion enhancement. Very recently, the first fusion data for a projectile having a proton halo in its ground state, in this case the ^{8}B + ^{58}Ni system, were reported [7]. In contrast to the case of the neutron-halo projectile, the latter system shows a fusion enhancement at all measured energies, even above the barrier. This result was unexpected, especially because the total reaction cross sections behave similarly for both neutron-halo and proton-halo systems. Indeed, it has been shown that the reduced total reaction cross sections for ^{8}B + ^{58}Ni and for several neutron-halo systems fall on the same trajectory when plotted as a function of the reduced energy [8].

It would seem then that, while the charged nature of the proton halo is not important to determine total reaction probabilities, it does make a difference when the fusion process is isolated. Within this context, the possible role of the charge excess of the projectile can be tested by making fusion measurements for other proton-rich nuclei. The ^{7}Be nucleus is an interesting case study. In addition to lying on the proton-rich side of the line of nuclear stability, it is weakly bound with a separation energy of 1.59 MeV for breakup into ^{3}He and ^{4}He. ^{7}Be is a radioactive nucleus with a half-life of 53.2 d and it is the core for the proton-halo nucleus ^{8}B.

*eli.aguilera@inin.gob.mx
†Present address: Instituto de Física, Universidade Federal Fluminense, Av. Litoranea s/n, Gragoatá, Niterói, R. J., 24210-340, Brazil.
‡Present address: Los Alamos National Lab, Los Alamos, New Mexico, 87545, USA.
§Deceased.
‖Present address: Department of Physics, and Astronomy and Cyclotron Institute, Texas A&M University, College Station, Texas, 77843, USA.
¶Present address: Physics Department, University of Minnesota, Minneapolis, Minnesota, 55455, USA.
**Present address: 21st Century Oncology, 555 D'onofrio Dr, Madison, Wisconsin, 53719, USA.

TABLE I. Experimental details. E_{in} is the incident energy (in the laboratory system) while $E_{c.m.}$ is the effective energy for fusion in the center-of-momentum frame of reference. In contrast to E_{in}, $E_{c.m.}$ includes energy-loss corrections properly weighted by the slope of the fusion excitation function.

Stage	Tgt. thick. (mg/cm^2)	Tgt. size (cm)	Bkwd. telescopes (deg)	Monitors (deg)	E_{in} (MeV)	$E_{c.m.}$ (MeV)
1	1.36	2.5 (diam.)	120, 135, 150	45, 60[a]	20.1	17.4
					21.9	19.0
2	5.60	13 × 13	113, 128, 143, 158	±45[b]	16.4	13.9
3	2.22	8.9 × 8.9	113, 128, 143, 158	±45[b]	17.5	15.0
					19.4	16.6
					20.9	17.9

[a] E-ΔE telescopes.
[b] Single detectors.

It is worth mentioning that, except for ^{8}B + ^{58}Ni, no weakly bound system has been reported to display a total fusion enhancement above the barrier. The extensive systematics for weakly bound systems covered in Refs. [5,6,9] seems to indicate that, except for neutron-halo systems, the total fusion cross sections above the barrier are not enhanced or suppressed but coincide with expectations. Below the barrier, most weakly bound systems appear to present an enhancement with respect to a standard reference (see Sec. IV).

In an attempt to further understand the most relevant reaction mechanisms involved in the interaction of weakly bound systems, in this work the evaporation proton yields for ^{7}Be + ^{58}Ni are measured at energies near and below the barrier. By inferring then the respective fusion yields, the results can help to clarify whether the proton excess plays a role in enhancing the fusion process at energies near the barrier.

The experimental procedure and results are described in Sec. II. In Sec. III, the data are compared with barrier-penetration-model calculations and with coupled-channel calculations where the most relevant inelastic channels are taken into account. In Sec. IV, the results are compared with other fusion measurements for ^{7}Be projectiles. Finally, a summary and the conclusions of this work are presented in Sec. V.

II. EXPERIMENTAL PROCEDURE AND RESULTS

The present experiment is part of an extensive project in which the *TwinSol* radioactive nuclear beam facility [10] at the University of Notre Dame (UND) was used to produce a mixed secondary beam of ^{8}B, ^{7}Be, and ^{6}Li. This beam was focused by *TwinSol* and used to bombard Ni targets, measuring in each case the respective protons evaporated after the corresponding fusion reaction. A bunched beam was used to separate the reaction products corresponding to each beam component by time of flight (TOF). A concise description of the general experimental procedure is given in Ref. [7], where the results for the fusion of ^{8}B + ^{58}Ni were reported. The specific details related to the ^{7}Be data are described here.

The ^{7}Be isotope was generated by means of the one-proton transfer reaction ^{3}He(^{6}Li,^{7}Be). Secondary beam rates (at target) of 0.5–1.2 × 10^5 particles/s were produced using primary ^{6}Li^{3+} beams with energies between 31 and 38 MeV delivered by the UND FN tandem accelerator, which produced ^{7}Be beams with the energies indicated in column E_{in} of Table I. Three or four ΔE-E silicon surface-barrier telescopes were used at backward angles to detect the protons evaporated from the fused system. Two additional telescopes (or single detectors) placed at forward angles served to monitor the beam. To compensate for the low beam rates for bunched beams at *TwinSol*, fairly thick natural Ni targets were used and the experiment was performed in three stages. These stages, ordered chronologically, are described in Table I along with respective experimental details. Except in stage one, the thin (ΔE) detectors of the backward telescopes had a typical thickness of ∼40 μm. For stage one, they were 65–95 μm thick, while the respective thickness of the monitor ΔE detectors was ∼20 μm. The thick (E) detectors were typically ∼1000 μm thick, except for those in the monitors at stage two whose thickness was 150 μm. Collimators of 18–25 mm diameter were placed in front of all telescopes and monitors.

A sample beam spectrum, corresponding to the E_{in} = 19.4 MeV run, is shown in Fig. 1. The secondary beam energy width [full width at half maximum (FWHM)] varied between 0.7 and 1 MeV, while the respective time resolution was between 7 and 12 ns. Note that the three main components

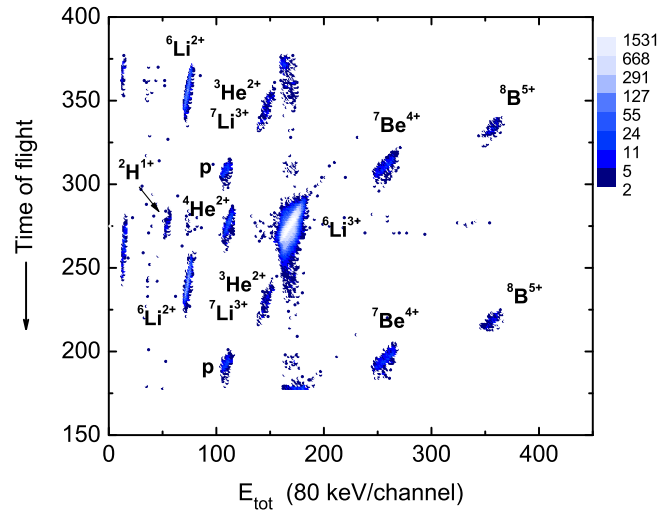

FIG. 1. (Color online) Secondary beam composition. Data shown taken with a detector temporarily placed at the target position after lowering the beam rate by three orders of magnitude.

of the mixed beam (^{8}B, ^{7}Be, and ^{6}Li) are well separated from each other by TOF, but each one has its own contaminants (having the same TOF), which must be dealt with separately. A major concern in the present experiment was the presence of a satellite proton beam with the same TOF as the ^{7}Be (see Fig. 1) which could potentially mask the protons of interest. However, in the backward telescopes the respective elastic peak lies above the high-energy tail of the proton spectra corresponding to fusion-evaporation for ^{7}Be + ^{58}Ni. Therefore, the contaminant protons could be properly discriminated against by their energy. For some runs the satellite proton beam was not well focused and grazed the target frame. The consequent thick-target yield of backscattered protons prevented clean identification of proton-evaporation events for these runs so they were not included in the present report.

The effective beam spot size at target was checked by placing a telescope, with a position-sensitive E detector (PSD), at the position of the target. The typical FWHM was ~10 mm, which is much smaller than the target size (see Table I). However, even a faint beam-halo interacting with the target frame can produce substantial amounts of undesirable background (bkg.) protons that reach the telescopes. These bkg. problems were partially solved by increasing the size of the target frames, originally with circular bores of 2.5 cm diameter, to square frames with internal side lengths of 13 and 8.9 cm (Table I). In addition, background determinations were performed for these larger targets by using pairs of identical target frames, one with no target. Blank-target measurements were done immediately after the respective runs with a Ni target with no modification of the setup or the beam conditions. Typically, bkg. contributions were negligible for these big target frames. For the runs with the smaller target (stage 1), clear evidence for bkg. problems appeared in the data but no actual background measurements were performed. Instead, an interpolation between the points corresponding to the two largest energies in stage 3 was used to renormalize the $E_{\mathrm{c.m.}} = 17.4$ MeV point and the same normalization factor was then applied to the $E_{\mathrm{c.m.}} = 19.0$ MeV point. Under the reasonable assumption that the ratio of background to total proton yields is similar for the two energies, this should be a good approximation. In addition, a possible 10% error in this ratio was convoluted in the uncertainty assigned to the higher-energy point.

A typical proton spectrum is presented in Fig. 2, along with the predictions of the evaporation code PACE2 [11]. A good agreement is observed, indicating consistency of the data with the expectations for evaporated protons.

Fusion cross sections were extracted from the measured proton yields through the corresponding multiplicities calculated with the code PACE2 [11]. According to this code, between 97% and 99% of the fusion-evaporation events contain at least one proton for the measured bombarding energies. Thus, evaporation protons are a good signature for fusion. Appropriate corrections were introduced to account for the respective isotopic composition of the natural Ni targets. The validity of this type of correction was verified in Ref. [7] for a ^{8}B beam by comparing with equivalent measurements with an enriched ^{58}Ni target. Table II presents both the experimental proton cross sections and the derived fusion cross sections, along with the respective proton multiplicities.

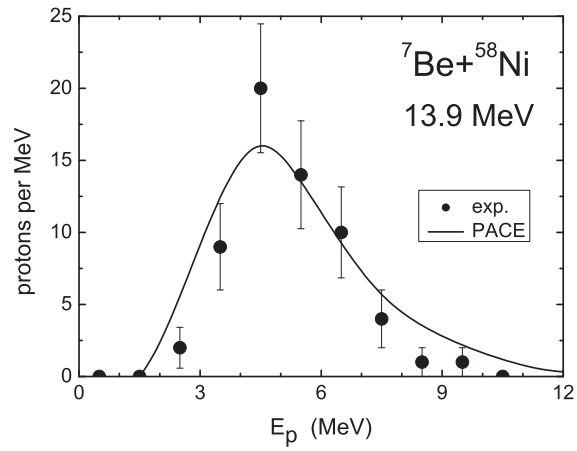

FIG. 2. Typical proton spectrum, obtained by summing the data for the telescopes at 113, 143, and 158 deg.

In the present work, default values were used for most input parameters in PACE2. More specifically, the yrast line was always determined by the liquid-drop rotational energy, with the Sierk fission barrier assumed throughout the calculations, and the regular Wapstra mass table supplied with the code used for all involved nuclei. The level density parameter was $a = A/8.6$ (but the effect of variations in a was investigated; see below), which differs from the default value, $a = A/7.5$. The value of $A/8.6$ gives a better approximation to the measured densities in the region of $60 \leqslant A \leqslant 70$ [12], where the compound and residual nuclei lie for the present reaction. In addition, the experimental fusion cross sections were used as an input (in an iterative way), which means that the code internally shifts the respective optical model transmission coefficients to reproduce these values.

Model dependency was tested by analyzing the sensitivity of the calculated multiplicities to both the level densities and the respective transmission coefficients T_l involved. First, the level density parameter a was varied in PACE2 within the extreme values $A/9.5 \leqslant a \leqslant A/7.9$, which delimit the region of measured densities for the relevant nuclei ($60 \leqslant A \leqslant 70$) [12]. These changes produced a maximum variation of about 5% in the multiplicities. In PACE2, T_l's are calculated for the compound-nucleus values of A and Z and an extrapolation is

TABLE II. Integrated cross sections for evaporated protons (σ_p), proton multiplicities (M_p), and deduced fusion cross sections (σ_{fus}). Only statistical uncertainties are reported here. An additional 15% systematic uncertainty should be considered (see text).

E_{lab} (MeV)	$E_{\mathrm{c.m.}}$ (MeV)	σ_p (mb)	M_p	σ_{fus} (mb)
15.6	13.9	41.9 ± 5.0	1.61	26.0 ± 3.1
16.8	15.0	97.8 ± 11.0	1.60	61.1 ± 6.9
18.6	16.6	269.3 ± 52.5	1.63	165.2 ± 32.2
19.5	17.4	411.1 ± 131.1	1.67	246.2 ± 78.5
20.1	17.9	493.5 ± 77.1	1.69	292.0 ± 45.6
21.3	19.0	694.7 ± 203.9	1.76	394.7 ± 115.8

made for subsequent decays by assuming that the respective T_l values are shifted in their kinetic-energy dependence [13]. Additional multiplicity calculations with the code LILITA [14,15] also were performed where an explicit calculation of all necessary transmission coefficients is made [15]. The input parameters for LILITA were chosen so as to give a meaningful comparison with the respective PACE2 calculations. This yielded a maximum difference of 5% with respect to the results from PACE2. Based on the above results, an estimated systematic uncertainty of 7% can be assigned to the reported fusion cross sections (but see below).

The procedure used to derive the fusion cross sections is based on the assumption that complete fusion (CF) is the only mechanism responsible for the observed proton yields. However, as discussed below, it is safer to adopt the reported values for the total fusion cross sections. In the incomplete fusion (ICF) process, one of the residues ^{3,4}He after projectile breakup would be absorbed by the target. This would also produce evaporated protons, but with lower multiplicities than the CF case. Indeed, the respective PACE2 calculations indicate that these multiplicities are roughly 60% of those in Table II. More precisely, defining $r_A(E) = M_p(^A\mathrm{He})/M_p(^7\mathrm{Be})$, where M_p stands for the respective proton multiplicity, the mean values obtained in the relevant energy range are $r_A(E) = 0.62 \pm 0.04$ (0.59 ± 0.3) for $A = 3$ (4), respectively. For these calculations, the available energy for fusion of the respective fragments was estimated from the formula given in Ref. [16] after being adapted to the present case. If some fraction of the measured protons came from ICF, they should be mapped into σ_{fus} by using the decreased multiplicity, while the remaining fraction would still be mapped as done above. As a consequence, the total fusion (TF = CF + ICF) cross sections would yield values systematically larger than those reported in Table II. It is worth mentioning that the remaining ^{3,4}He residues that would not be absorbed after possible ICF would not go through the ΔE detectors of the backward telescopes so their presence could not be verified in these telescopes. However, evidence for these residues was found in the forward telescopes used as monitors in stage one and will be discussed later in Sec. IV.

Although the present experiment cannot distinguish CF from ICF, the previously reported data on total reaction cross sections [17] can help establish an upper bound for the possible contribution of ICF. Figure 3 shows such data along with the σ_{fus} values from Table II. The dotted line, drawn to guide the eye, defines a reasonably smooth trend for the σ_R points. It can be seen that the fusion yield nearly saturates the total reaction cross sections. At most, an additional 15% contribution to σ_{fus} could be allowed. It can be shown that such an increase would still be consistent with our data if ∼20% of the measured protons came from ICF and σ_{fus} (interpreted now as the total fusion cross section) is calculated by using the mixed multiplicities, as described above. This in turn would imply a ratio ICF/TF of ∼30% or, equivalently, a ratio CF/TF of ∼70%. Of course, this maximum contribution of ICF could be achieved only if inelastic and other direct processes, which do not produce protons at backward angles, have negligible cross sections in the measured energy region. Summarizing, whereas we cannot rule out the possibility of ICF, its presence would increase the reported values for σ_{fus} by at most 15% as long as they refer to total fusion. This would leave the values of σ_{fus} within the reported error bars for all energies except the two lowest ones, for which the error bars are ∼12%. For this reason, the σ_{fus} values reported in Table II are adopted for the total fusion cross sections, and we assign to them a 15% systematic error instead of the 7% value discussed earlier.

III. COMPARISON WITH CALCULATIONS

The dashed curve in Fig. 3 represents the fusion cross sections predicted for $^7\mathrm{Be} + ^{58}\mathrm{Ni}$ by the one-dimensional barrier-penetration model (BPM) of Wong [18]. The respective barrier parameters, obtained by using the São Paulo potential (SPP) [19] for the bare nuclear potential, are $V_B = 16.58$ MeV, $R_B = 8.96$ fm, and $\hbar\omega_0 = 3.79$ MeV. The barrier height is indicated by the vertical arrow in Fig. 3. Clearly, the experimental total fusion cross section shows an enhancement with respect to these predictions, even in the region above the barrier.

For light- and medium-mass systems such as $^7\mathrm{Be} + ^{58}\mathrm{Ni}$, it is well known that the assumptions involved in Wong's model break down at some point for energies below the barrier where the parabolic-barrier approximation ceases to be valid. To investigate this point, an optical model potential (OMP) calculation was done by using again the SPP for the real part with an interior imaginary potential of Woods–Saxon form, having parameters $W_0 = 50$ MeV, $r_W = 1.06$ fm, $a_W = 0.2$ fm. The absorption in this potential effectively simulates an incoming wave boundary condition, thus providing a good estimation for fusion. The results are represented by the solid line in Fig. 3. It was checked that they are fairly insensitive to respective variations in the parameters of the imaginary potential ($20 \leqslant W_0 \leqslant 100$; $0.8 \leqslant r_W \leqslant 1.06$; $0.1 \leqslant a_W \leqslant 0.3$). These results corroborate Wong's predictions above the barrier and indicate

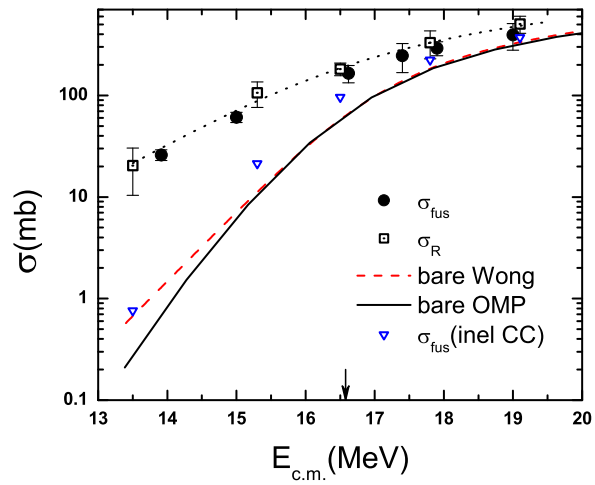

FIG. 3. (Color online) Fusion excitation function obtained for $^7\mathrm{Be} + ^{58}\mathrm{Ni}$ and respective total reaction data from Ref. [17]. The arrow marks the location of V_B for this system and the curves are explained in the text. The error bars include only statistical uncertainties. An additional 15% systematic uncertainty should be considered (see text).

that a noteworthy difference between the two calculations would appear only for the case of the measured point at the lowest energy.

To test for possible effects on fusion of inelastic channels, coupled channel (CC) calculations were performed for $E_{\rm lab} = 21.4$ MeV by using the optical potential previously described. Elastic-scattering data are available for this energy [17], which in addition is close to the highest fusion energy measured in the present work. By assuming a vibrational model for ^{58}Ni, inelastic excitation of the first 2^+ (1454 keV) and 3^- (4475 keV) states was included. The respective coupling strengths, very similar to the ones used in Ref. [20], were obtained from Refs. [21,22]. Excitation of the 429 keV $(1/2^-)$ state in ^{7}Be also was included by assuming for this nucleus a rotational model where both this and the respective ground state belong to the same $K = 1/2^-$ rotational band. The coupling strengths in this case were obtained from the value $B(E2; 3/2^- \rightarrow 1/2^-) = 18.9$ e^2 fm^4 reported in Ref. [23]. The code FRESCO [24] was used to perform the CC calculations. As done above, the fusion cross section was calculated from the total absorption in the short-range imaginary potential $W(r)$. The validity of the wave function used to calculate this absorption can be checked by comparing the respective predictions for the elastic-scattering angular distribution with the data.

The results for the elastic-scattering angular distribution are presented in Fig. 4, along with the respective data from Ref. [17]. The dash-dotted line corresponds to the single-channel calculation where no inelastic channels are considered. It yields a χ^2/N value of 4.8, which is fairly large due mainly to the poor description of the points near the region of the Coulomb rainbow. The dashed curve includes the effects of the full inelastic couplings for the target, yielding $\chi^2/N = 3.3$, which is a substantially improved value. Finally, the solid curve includes in addition the contribution of the inelastic scattering channel populating the $1/2^-$ state in ^{7}Be, which could not be resolved in the data of Ref. [17]. This increases slightly the cross section at backward angles, which improves the agreement with the data. Considering that these

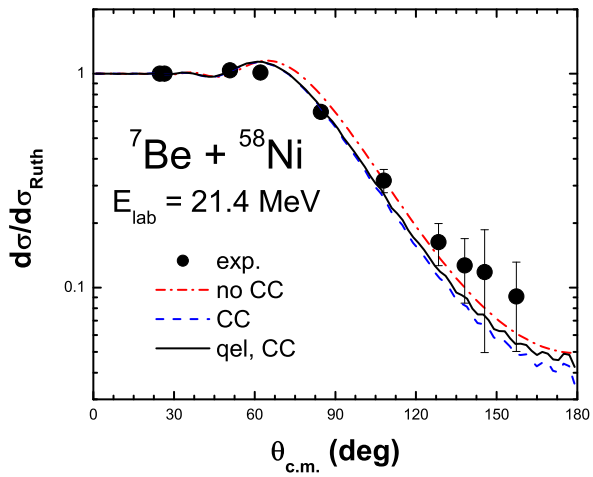

FIG. 4. (Color online) Elastic-scattering angular distribution for ^{7}Be + ^{58}Ni at $E_{\rm lab} = 21.4$ MeV. Data are from Ref. [17] while the curves correspond to FRESCO calculations described in the text.

calculations are completely parameter free, one can conclude that a good description of the data is achieved. In fact, the calculated total reaction cross section ($\sigma_R = 442$ mb) agrees with the value reported in Ref. [17] ($\sigma_R = 506 \pm 97$ mb) within uncertainties.

A few words are in order with respect to possible angle uncertainties in the data of Fig. 4, which were minimized in the experiments of Ref. [17] by using the following procedure: (a) The experimental setup included detectors placed at both sides of the beam direction, with several forward-angle detectors (where the measurements have a greater sensitivity to the angle); elastic scattering measurements with a gold target were done, which guarantees pure Rutherford scattering, thus allowing one to determine any possible angular offset with high precision. (b) Effective angles were calculated by applying an averaging procedure over the beam spot and the detector aperture, where the angles were weighted by the Rutherford formula. A Monte Carlo code was used that properly simulates the different beam rays exiting *TwinSol*, including the respective directions and energies and the beam spot size at the target. (c) Comparison of the experimental angular distribution for the Au target with the respective Rutherford curve did show very good consistency, within statistical uncertainties, implying negligible errors for the angles and thus validating the procedure. (d) For the measurements with the lower-Z Ni target, step (b) was repeated but the angles were weighted by using, instead of Rutherford's curve, a smooth curve fitting the experimental angular distribution, in an iterative way. With the above procedure, any remaining angular uncertainties can be safely neglected.

Breakup coupling calculations at a somewhat larger energy (24.1 MeV) were recently reported for this system [25], showing a considerable enhancement of the large-angle angular distribution for elastic scattering. This suggests that even better agreement with the data of Fig. 4 could probably be achieved by inclusion of the respective breakup couplings.

As for the fusion cross section, the value obtained is shown by the downward triangle at $E_{\rm c.m.} = 19.1$ MeV in Fig. 3. It represents a $\sim$16% enhancement with respect to the bare OMP calculation and is in good agreement with the experimental value corresponding to $E_{\rm c.m.} = 19$ MeV. The results of similar calculations at lower energies, that also were measured in the elastic-scattering experiments of Ref. [17], are also displayed in Fig. 3. The corresponding energies were $E_{\rm lab} = 19.2$, 18.5, 17.1, and 15.1 MeV and the χ^2/N values obtained when comparing the predictions for the elastic-scattering angular distributions with the data were 1.15, 0.96, 0.98, and 0.042, respectively. These reasonably low values of χ^2/N validate the respective wave functions used to calculate the corresponding absorption, i.e., the $\sigma_{\rm fus}$(inel CC) values shown in Fig. 3. With respect to the solid curve, increasingly higher enhancements are observed with decreasing energies due to the above inelastic couplings, but these results also indicate that additional channels will be needed to explain the very large fusion enhancements observed at lower energies. Possible effects of transfer, breakup and/or incomplete fusion also should be considered. More detailed calculations, which are beyond the scope of the present work, are necessary to properly describe the entire experimental fusion excitation function.

IV. COMPARISON WITH FUSION DATA FOR OTHER SYSTEMS WITH ^{7}BE PROJECTILES

For the purpose of comparing fusion data for different systems, we follow the prescription first proposed by Gasques *et al.* [26] and extensively studied by Canto *et al.* [5,6] in the context of weakly bound projectiles. In this approach, the barrier parameters V_B, R_B, $\hbar\omega_0$, are obtained from a realistic bare potential and used to reduce the cross section and the energy through the expressions:

$$F(x) = \frac{2E}{\hbar\omega_0 {R_B}^2}\sigma, \quad x = \frac{E - V_B}{\hbar\omega_0}. \tag{1}$$

In order to decide whether the data present enhancement or suppression, the reduced cross sections can then be compared with the so-called universal fusion function (UFF),

$$F_0(x) = \frac{2E}{\hbar\omega_0 {R_B}^2}\sigma^W = \ln[1 + e^{(2\pi x)}], \tag{2}$$

where σ^W stands for the expression derived for the cross section in the one-dimensional barrier penetration model of Wong [18]. To avoid possible inaccuracies in Wong's model, such as those mentioned in connection with Fig. 3, the cross sections are renormalized with respect to the corresponding OMP calculations (solid curve in Fig. 3) and the result is multiplied by $F_0(x)$ (see Refs. [5,6,26]). In other words, instead of just using Eq. 1, the data are reduced according to the expression $(\sigma_{\rm expt}/\sigma_{\rm OMP})F_0(x)$. With this reduction, it is reasonable to compare the reduced data for different systems directly on the same plot, still using $F_0(x)$ as a standard reference even though Wong's model might fail for some data. We used always the double-folding São Paulo potential (SPP) [19] to derive the barrier parameters, with default values for the matter and charge densities. These densities follow the systematics observed for many nuclei. With this procedure, any deviations from the reference curve can in principle be ascribed either to static effects, related to deviations in the actual densities, or to dynamic effects, associated with some intrinsic properties of the involved nuclei.

In addition to the present data, fusion measurements with ^{7}Be projectiles have been performed for the lighter target ^{27}Al [27] and for the much heavier target ^{238}U [28]. Table III shows the barrier parameters used for each system, and the corresponding reduced results are presented in Fig. 5. To make this figure, the imaginary potential mentioned in Sec. III ($W_0 = 50$ MeV, $r_W = 1.06$ fm, $a_W = 0.2$ fm) was used to calculate $\sigma_{\rm OMP}$ for all systems. Sensitivity tests to the parameter values similar to the ones mentioned above for the Ni case were also met by the systems with the Al and U targets.

TABLE III. Barrier parameters obtained from the São Paulo potential for the several systems.

System	V_B (MeV)	R_B (fm)	$\hbar\omega_0$ (MeV)
^{7}Be + ^{27}Al	8.35	8.21	3.09
^{7}Be + ^{58}Ni	16.58	8.96	3.79
^{7}Be + ^{238}U	43.17	11.49	5.23

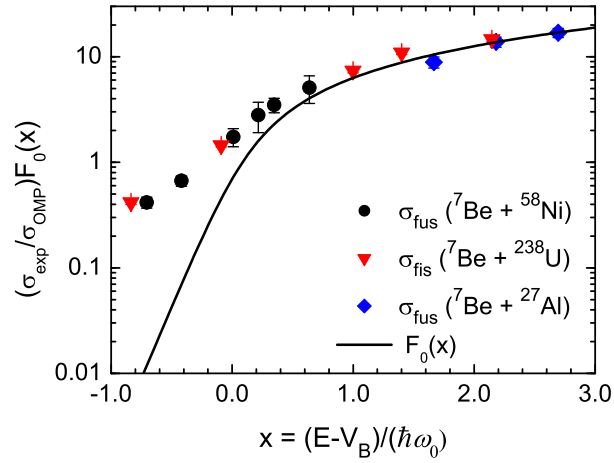

FIG. 5. (Color online) Comparison of reduced data for ^{7}Be projectiles with targets of ^{58}Ni (present work), ^{238}U [28], and ^{27}Al [27]. The curve corresponds to the UFF.

It is worth mentioning that the renormalization involving $\sigma_{\rm OMP}$ affected mainly the lowest-energy points for the U and Ni targets. To be more specific, if the data reduction of Eq. (1) had been used, with no renormalization, Fig. 5 would look quite similar except by the lowest-energy points for Ni and U, which would appear lowered by factors of 2.7 and 1.9, respectively.

The points for the ^{238}U target actually correspond to the total fission cross sections, $\sigma_{\rm fis}$, measured in Ref. [28]. As the authors point out, in addition to complete fusion these cross sections would also include contributions from any process where a compound system is formed with excitation energy above the corresponding fission threshold. In addition to CF, ^{3}He or ^{4}He direct transfer to highly excited states, as well as possibly incomplete fusion, were identified in Ref. [28] as the most probable processes. In the context of the present measurements with the Ni target, such processes, if present, also would contribute to the evaporated protons. We believe for this reason that in this case our data should be compared to $\sigma_{\rm fis}$ rather than comparing them to the complete fusion data that were reported in Ref. [28].

It is quite interesting that, in spite of the huge mass and charge differences in the targets (^{58}Ni vs ^{238}U), both data sets follow the same trend in the region where the respective reduced energies overlap. This could indicate that the dominant mechanism responsible for the large sub-barrier enhancement in both cases is mainly associated with the ^{7}Be projectile, independent of the target. In the case of the ^{7}Be + ^{238}U system, coincidence measurements of fission and light particles, along with proper kinematic considerations, indicate that direct transfer (or ICF) of ^{3,4}He are the most probable mechanisms contributing to fission in the sub-barrier region [28]. It would be interesting to investigate the possible importance of these mechanisms in the case of the ^{7}Be + ^{58}Ni system. Although the present experiment was not designed to measure transfer or breakup residues, the forward telescopes used in stage one (Table I) served to check for the possible presence of ^{3,4}He at 45 and 60 degrees for the corresponding energies (17.4 and

19 MeV). A global survey of the respective data did certainly confirm the presence of these isotopes. At 19 MeV, the sum of yields at the two detectors gave approximately 15 mb/sr for both isotopes, while at 17.4 MeV this sum gave cross-section values of ∼29 mb/sr for ^{3}He and ∼66 mb/sr for ^{4}He. One can speculate that the larger yields observed for ^{4}He might indicate a net absorption of ^{3}He by the target, possibly related to ICF with ^{3}He or direct transfer of this cluster. Further experiments are needed to corroborate this hypothesis.

The data for the ^{27}Al target were taken at much higher reduced energies than ours, but they do overlap in energy with one point for ^{238}U. In contrast to the latter, the points for the former system show a small suppression with respect to the reference curve. The lowest-energy point for the light system, in particular, clearly falls below the trend defined by the two neighboring ^{238}U points. These ^{27}Al data were obtained in Ref. [27] by subtracting the measured one-proton-stripping cross sections from the total reaction data deduced from respective quasielastic scattering measurements. Clearly, it should be correct to associate the reported points to the total fusion cross section or, at worst, to an upper bound for it. As a matter of fact, these data were included also in a systematic comparison [9] of TF data for several weakly bound projectiles (^{6,7}Li, ^{7,9}Be) with ^{27}Al and ^{28}Si targets. A small suppression similar to that in Fig. 5 is also seen for the ^{7}Be + ^{27}Al data in that comparison, with respect to the rest of the systems, despite the fact that possible effects of target and/or projectile excitation were taken into account in Ref. [9]. The discrepancy is relatively small, though, and will not be discussed here any further.

V. SUMMARY AND CONCLUSIONS

Fusion cross sections for the ^{7}Be + ^{58}Ni system were extracted from evaporated-proton measurements at six near-barrier energies. Arguments are given showing that, by assigning an appropriate systematic uncertainty, the reported cross sections can be safely associated with TF. Strictly speaking, they would include contributions from any process producing nuclei excited to energies above the respective proton emission threshold. In cases where direct reactions such as ^{3,4}He transfer prove to be important in this context, the definition of TF would need to be extended to include them, as has been done in other works (see Ref. [29] and references therein).

The data show a large sub-barrier enhancement with respect to expectations for a bare potential, with lower but still sizable enhancements above the barrier. Up to some degree, this is similar to the situation observed for ^{8}B + ^{58}Ni [7] except that the enhancement persists at even higher energies above the barrier for the latter system [30]. CC calculations for the present system indicate that, at the higher energies measured, inelastic couplings may account for most of the observed enhancement, but additional channels need to be considered at lower energies.

A comparison with available data for ^{7}Be on a ^{238}U target shows a nice agreement between the respective reduced data as long as total fission is considered for the latter target. The validity of this comparison may be qualitatively substantiated because both measured processes, fission and proton evaporation, require the formation of a compound system with excitation energy above a threshold, i.e., the fission and the proton emission threshold, respectively. The similar behavior found at low energies for both the ^{58}Ni and the ^{238}U targets suggests that some process related to the ^{7}Be projectile may be the main process responsible for the observed enhancement. According to the measurements of Ref. [28], such a process would most probably be either the direct transfer of ^{3,4}He or ICF with one of these clusters. Some evidence concerning the possible presence of these processes in the present experiment also is presented. Reduced total fusion data for the ^{7}Be + ^{27}Al system were also compared. With small, probably unimportant, discrepancies the respective experimental points seem to also follow the general trend defined by the data for the ^{58}Ni and ^{238}U targets.

ACKNOWLEDGMENTS

E.F.A. is grateful for useful discussions with Antonio Moro as well as for the warm hospitality of all personnel at Notre Dame during the measurements. This work has been partially supported by CONACYT (México) and by NSF (USA) under Grants No. PHY09-69456 and No. PHY-0969058.

[1] L. F. Canto, P. R. S. Gomes, R. Donangelo, and M. S. Hussein, Phys. Rep. **424**, 1 (2006).
[2] N. Keeley, R. Raabe, N. Alamanos, and J. L. Sida, Prog. Part. Nucl. Phys. **59**, 579 (2007).
[3] A. S. Fomichev, I. David, Z. Dlouhy, S. M. Lukyanov, Yu. Ts. Oganessian, Yu. E. Penionzkevich, V. P. Perelygin, N. K. Skobelev, O. B. Tarasov, and R. Wolski, Z. Phys. A: Hadrons Nucl. **351**, 129 (1995).
[4] J. J. Kolata *et al.*, Phys. Rev. Lett. **81**, 4580 (1998).
[5] L. F. Canto, P. R. S. Gomes, J. Lubian, L. C. Chamon, and E. Crema, J. Phys. G **36**, 015109 (2009).
[6] L. F. Canto, P. R. S. Gomes, J. Lubian, L. C. Chamon, and E. Crema, Nucl. Phys. A **821**, 51 (2009).
[7] E. F. Aguilera *et al.*, Phys. Rev. Lett. **107**, 092701 (2011).
[8] J. J. Kolata and E. F. Aguilera, Phys. Rev. C **79**, 027603 (2009).
[9] P. R. S. Gomes, J. Lubian, and L. F. Canto, Phys. Rev. C **79**, 027606 (2009).
[10] M. Y. Lee *et al.*, Nucl. Instrum. Methods Phys. Res., Sect. A **422**, 536 (1999).
[11] A. Gavron, Phys. Rev. C **21**, 230 (1980).
[12] R. G. Stokstad, in *Treatise on Heavy-Ion Science*, edited by D. A. Bromley (Plenum Press, New York, 1985), Vol. 3, p.83.
[13] A. Gavron, in *Computational Nuclear Physics 2; Nuclear Reactions*, edited by K. Langanke, J. A. Maruhn, and S. E. Koonin (Springer, New York, 1993), p. 108.
[14] J. Gomez del Campo and R. G. Stokstad, ORNL Report TM-7295 (1981).
[15] J. Gomez del Campo (private communication).
[16] E. F. Aguilera, E. Martinez-Quiroz, P. Rosales, J. J. Kolata, P. A. DeYoung, G. F. Peaslee, P. Mears, C. Guess, F. D. Becchetti, J. H. Lupton, and Yu Chen, Phys. Rev. C **80**, 044605 (2009).

[17] E. F. Aguilera, E. Martinez-Quiroz, D. Lizcano, A. Gómez-Camacho, J. J. Kolata, L. O. Lamm, V. Guimarães, R. Lichtenthäler, O. Camargo, F. D. Becchetti, H. Jiang, P. A. DeYoung, P. J. Mears, and T. L. Belyaeva, Phys. Rev. C **79**, 021601(R) (2009).
[18] C. Y. Wong, Phys. Rev. Lett. **31**, 766 (1973).
[19] L. C. Chamon, B. V. Carlson, L. R. Gasques, D. Pereira, C. De Conti, M. A. G. Alvarez, M. S. Hussein, M. A. Cândido Ribeiro, E. S. Rossi, Jr., and C. P. Silva, Phys. Rev. C **66**, 014610 (2002).
[20] N. Keeley, J. S. Lilley, and J. A. Christley, Nucl. Phys. A **603**, 97 (1996).
[21] S. Raman, C. W. Nestor, Jr., and P. Tikkanen, At. Data Nucl. Data Tables **78**, 1 (2001).
[22] M. R. Bhat, Nucl. Data Sheets **80**, 789 (1997).
[23] N. Keeley, K. W. Kemper, and K. Rusek, Phys. Rev. C **66**, 044605 (2002).
[24] I. J. Thompson, Comput. Phys. Rep. **7**, 167 (1988).
[25] N. Keeley, R. S. Mackintosh, and C. Beck, Nucl. Phys. A **834**, 792c (2010).
[26] L. R. Gasques, L. C. Chamon, D. Pereira, M. A. G. Alvarez, E. S. Rossi, Jr., C. P. Silva, and B. V. Carlson, Phys. Rev. C **69**, 034603 (2004).
[27] K. Kalita *et al.*, Phys. Rev. C **73**, 024609 (2006).
[28] R. Raabe, C. Angulo, J. L. Charvet, C. Jouanne, L. Nalpas, P. Figuera, D. Pierroutsakou, M. Romoli, and J. L. Sida, Phys. Rev. C **74**, 044606 (2006).
[29] Y. D. Fang *et al.*, Phys. Rev. C **87**, 024604 (2013).
[30] E. F. Aguilera, E. Martinez-Quiroz, P. Amador-Valenzuela, A. Gómez-Camacho, and J. J. Kolata, J. Phys.: Conf. Ser. **492**, 012002 (2014).